Taylor series expansions for airborne radar space-time adaptive processing

Sophie Beau, Sylvie Marcos

Taylor series expansions for airborne radar STAP

Sophie Beau and Sylvie Marcos

Laboratoire des Signaux et Systèmes (LSS)
CNRS UMR8506, Université Paris Sud, SUPELEC
3 rue Joliot Curie, Plateau de Moulon, 91192 GIF-sur-YVETTE cedex, FRANCE
{beau, marcos}@lss.supelec.fr

Abstract

Space time adaptive processing (STAP) for range dependent clutter rejection in airborne radar is considered. Indeed, radar antenna architectures or configurations which are different from the conventional uniform linear antenna array (ULA) and side-looking configuration have consequences on the clutter properties. We here investigate the use of Taylor series expansions of the space-time covariance matrix in the classical sample matrix inversion (SMI) STAP method in order to mitigate the range non-stationarity of the clutter and we compare it to the Derivative Based Updating (DBU) already proposed in the literature. We also propose a new algorithm based on a Taylor series expansion of the clutter plus noise subspace in conjunction with the eigencanceler-based (EC) STAP, which improves the performance in term of SINR loss, compared to the DBU method. In this paper, the particular cases of a ULA and a uniform circularly curved antenna (UCCA) array in side-looking and non side-looking monostatic configurations as well as a ULA in some bistatic configurations are considered for the test and the comparison of the presented algorithms.

Index Terms

Pulse Airborne radar, Radar clutter, STAP, Taylor series expansion, range non stationarity, eigencanceler-based methods

Acronysms

$AADC$	$Adaptive\ Angle\ Doppler\ Compensation$
ADC	$Angle\ Doppler\ Compensation$
CME	$Covariance\ Matrix\ Expansion$
CNR	$Clutter-to-Noise\ Ratio$
CPI	$Coherent\ Processing\ Interval$
DD	$Doppler\ Direction$
DBU	$Derivative\ Based\ Updating$
DL	$Diagonal\ Loading$
DW	$Doppler\ Warping$
EC	$EigenCanceler$
NSL	$Non\ Side\ Looking$
$PICM$	$Prediction\ of\ Inverse\ Covariance\ Matrix$
PRI	$Pulse\ Repetition\ Interval$
PSD	$Power\ Spectral\ Density$
$RADAR$	$RAdio\ Detection\ And\ Ranging$
RDC	$Registration\ based\ range\ Dependence\ Compensation$
SE	$Subspace\ Expansion$
$SINR$	$Signal-to-Interference\ plus\ Noise\ Ratio$
SL	$Side-Looking$
SMI	$Sample\ Matrix\ Inversion$
SNR	$Signal-to-Noise\ Ratio$
$STAP$	$Space\ Time\ Adaptive\ Processing$
TSE	$Taylor\ Series\ Expansion$
ULA	$Uniform\ linear\ array$
$UCCA$	$Uniform\ Circularly\ Curved\ Array$

I. INTRODUCTION

Detection of slow moving targets with an airborne radar is a difficult task since they are masked by the ground clutter generated by the radar platform motion. Space-time adaptive processing (STAP) consists in mitigating the ground clutter by filtering the radar echoes received on a multiple antenna array for different coherent time pulses [1]-[4].

At a given range from the radar, the received signal can be written as the sum of the target component $\mathbf{x}_\mathrm{t}$ (when it is present at this range), the noise $\mathbf{x}_\mathrm{n}$ and the clutter $\mathbf{x}_\mathrm{c}$ components (we here suppose the absence of jammer). The optimum space-time filter at range k is given by $\mathbf{w}_k = \mathbf{R}_k^{-1}\mathbf{x}_\mathrm{t}$ where $\mathbf{R}_k = \mathrm{E}\left\{\mathbf{x}_k\mathbf{x}_k^H\right\}$ is the clutter plus noise covariance matrix and $\mathbf{x}_k = \mathbf{x}_{\mathrm{c},k} + \mathbf{x}_{\mathrm{n},k}$. We suppose that these two components are mutually uncorrelated such that $\mathbf{R}_k = \mathbf{R}_{\mathrm{c},k} + \sigma^2\mathbf{I}$ where $\mathbf{R}_{\mathrm{c},k}$ is the clutter covariance matrix at range k and σ^2 is the noise variance (the noise is assumed to be spatially and temporally white). The computation of this filter thus requires the estimation of the clutter plus noise covariance matrix. This is classically achieved using K snapshots at neighboring ranges

$$\hat{\mathbf{R}}_k = \frac{1}{K}\sum_{l=1,l\neq k}^{K}\mathbf{x}_l\mathbf{x}_l^H \tag{1}$$

yielding the sample matrix inversion (SMI) [5] algorithm for the STAP filter

$$\mathbf{w}_k^{SMI} = \hat{\mathbf{R}}_k^{-1}\mathbf{v}_\mathrm{t} \tag{2}$$

where $\mathbf{v}_\mathrm{t}$ is the target steering vector. It is shown in [5] that an average performance loss of 3 dB compared to the optimum can be obtained with $K = 2MN$, where M and N are the number of pulses and the number of antenna elements, respectively, when the snapshots are independent and identically distributed (iid) over ranges. This happens in the very particular case of a uniform linear antenna array (ULA) with a side-looking (SL) (the platform velocity vector is collinear with the antenna axis) monostatic (the receiver and the transmitter are colocated on the same platform) configuration which is classically used in the literature. Indeed, this case provides a certain redundancy of the data which implies some properties on the clutter space-time covariance matrix and a range stationarity of the neighboring snapshots. In this case only, the locus of the repartition of the power spectral density (PSD) of the clutter, namely, the locus of the clutter ridges, forms a straight line in the direction-Doppler (DD) (spatial frequency, Doppler frequency) plane. These DD curves overlap for all ranges but their length is reduced

when the range is reduced. However, in practice, whether in the presence of wind implying a crab angle between the platform direction and the ULA axis [6] or in the case of non ULA antenna arrays [7] or also in the case of bistatic radar (the transmitter and the receiver are not on the same platform) [8], the clutter ridges are no longer straight lines and, above all, become range dependent making the neighboring data non stationary in range and not iid. It then follows that the STAP weight vector in (2) is range dependent.

A number of methods in the literature have been devoted to the compensation of the clutter range dependency in STAP. Among the parametric methods are the Doppler Warping (DW) method [6][9], the Angle Doppler Compensation (ADC) method [10][11] and the Adaptive Angle Doppler Compensation (AADC) [11][12]. The derivative based updating (DBU) method [13], the Prediction of inverse covariance matrix (PICM) [14] and the Registration Based range dependence Compensation (RBC) [15][16] are non parametric methods in the sense that they do not require the knowledge of the radar configuration parameters.

In the DBU method, the weight vector is constructed at each range according to a first order Taylor series expansion (TSE) whose values are computed from an extended covariance matrix of the data. A TSE approach has also been presented for tracking non stationary (in time) signal sources by sensor array processing [17]. In the present paper, we will focus on this kind of TSE-based methods. Following [17], we will first introduce the TSE of the space-time covariance matrix in the SMI method yielding the covariance matrix expansion-based SMI (CME-SMI) method in order to mitigate the effects of the range dependency of the locus of the clutter ridges, it is to say the range non stationarity of the data. We will then establish the relationship and the difference between the CME-SMI and the DBU methods and we will conclude that the CME-SMI method encounters the same drawbacks as the SMI in a range non stationary context. Next, by introducing a TSE of the clutter and noise subspaces into the eigencanceler (EC) STAP algorithm [18], we will propose a new subspace expansion-based EC algorithm (SE-EC).

The performance of the proposed algorithm compared to the SMI, EC, DBU, CME-SMI and also SMI with diagonal loading (DL) will be then illustrated in the particular cases of a ULA array and a uniform circularly curved antenna array (UCCA) in a non side-looking monostatic configuration and a ULA array in some bistatic configurations.

The different Taylor series expansions applied to STAP are investigated and compared in section II. In section III, the locus of the clutter ridges, namely the DD curves, are analyzed and

discussed in both the above cited ULA and UCCA monostatic cases and in some bistatic cases. Section IV exhibits the simulation contexts and results. Section V is the conclusion.

II. STAP USING TAYLOR SERIES EXPANSION

A. Covariance Matrix Expansion-based SMI (CME-SMI)

The space time covariance matrix at range k can be expanded as[1]

$$\mathbf{R}_k = \mathbf{R}_{\mathrm{o}} + k\mathbf{\Delta R}_{\mathrm{o}} + o(k\mathbf{\Delta R}_{\mathrm{o}}) \tag{3}$$

where $\mathbf{R}_{\mathrm{o}}$ and $\mathbf{\Delta R}_{\mathrm{o}}$ are the clutter plus noise covariance matrix and the clutter plus noise derivative covariance matrix at range 0, respectively, and $o(k\mathbf{\Delta R}_{\mathrm{o}})$ a quantity negligible compared to $k\mathbf{\Delta R}_{\mathrm{o}}$.

The optimal STAP weight vector can then be approximated by

$$\mathbf{w}_k \approx \left(\mathbf{R}_{\mathrm{o}} + k\mathbf{\Delta R}_{\mathrm{o}}\right)^{-1}\mathbf{v}_{\mathrm{t}} \tag{4}$$

All the difficulty lies now into the estimation of $\mathbf{R}_{\mathrm{o}}$ and $\mathbf{\Delta R}_{\mathrm{o}}$. [17] proposes the following interpolation method. Rewriting (1) and taking its expectation yields

$$\mathrm{E}\left\{\hat{\mathbf{R}}_k\right\} = \frac{1}{K}\sum_{l=1,l\neq k}^{K}\mathbf{R}_l \approx \mathbf{R}_{\mathrm{o}} + k\mathbf{\Delta R}_{\mathrm{o}} \tag{5}$$

where$\mathbf{R}_l = \mathrm{E}\left\{\mathbf{x}_l\mathbf{x}_l^H\right\}$.

Using this equality at different range cells $k_1, \ldots k_E$, a least square estimation of $\mathbf{R}_{\mathrm{o}}$ and $\mathbf{\Delta R}_{\mathrm{o}}$ yields

$$\begin{bmatrix} \mathbf{R}_{\mathrm{o}} \\ \mathbf{\Delta R}_{\mathrm{o}} \end{bmatrix} \approx \left((\mathbf{T}^H\mathbf{T})^{-1}\mathbf{T}^H \otimes \mathbf{I}\right) \begin{bmatrix} \mathrm{E}\left\{\hat{\mathbf{R}}_{k_1}\right\} \\ \ldots \\ \mathrm{E}\left\{\hat{\mathbf{R}}_{k_E}\right\} \end{bmatrix} \tag{6}$$

where $\mathbf{I}$ is the $NM \times NM$ identity matrix and

$$\mathbf{T} = \begin{bmatrix} 1 & k_1 \\ \ldots & \\ 1 & k_E \end{bmatrix} \tag{7}$$

[1]To keep an acceptable complexity, we are only interested in first order expansions.

It is proposed in [17] to replace the expectations $\mathrm{E}\left\{\hat{\mathbf{R}}_{k_i}\right\}$ in (6) by single realizations $\hat{\mathbf{R}}_{k_i}$ given by (1) for $k = k_i$, to estimate $\mathbf{R}_{\mathrm{o}}$ and $\mathbf{\Delta R}_{\mathrm{o}}$. The difficulty of this approach amounts to that of the standard SMI, it is to say, the estimation of the covariance matrix $\mathbf{R}_{k_i}$ in a range non stationary context. Indeed, we will observe in the simulation section that the CME-SMI and the SMI without any range compensation yield similar results.

Let us now recall the DBU method and investigate its relationship and difference with the CME-SMI method.

B. Taylor series expansion of the weight vector (DBU)

The DBU [13] is based on the first order development of the STAP weight vector at range k given by

$$\mathbf{w}_k \approx \mathbf{w}_{\mathrm{o}} + \alpha_k \mathbf{\Delta w}_{\mathrm{o}} \tag{8}$$

The output of the STAP filter is $\mathbf{w}_k^H \mathbf{x}_k \approx \tilde{\mathbf{w}}^H \tilde{\mathbf{x}}_k$, where the extended weight vector and the extended data vector are

$$\tilde{\mathbf{w}} = \begin{bmatrix} \mathbf{w}_{\mathrm{o}} \\ \mathbf{\Delta w}_{\mathrm{o}} \end{bmatrix} \tag{9}$$

and

$$\tilde{\mathbf{x}}_k = \begin{bmatrix} \mathbf{x}_k \\ \alpha_k \mathbf{x}_k \end{bmatrix} \tag{10}$$

respectively. The DBU range compensation method thus consists in finding $\mathbf{w}_{\mathrm{o}}$ and $\mathbf{\Delta w}_{\mathrm{o}}$ of (8) through the optimum extended weight vector

$$\tilde{\mathbf{w}} = \mathbf{R}_E^{-1} \begin{bmatrix} \mathbf{v}_{\mathrm{t}} \\ \mathbf{0} \end{bmatrix} \tag{11}$$

where

$$\mathbf{R}_E = \mathrm{E}\left\{\tilde{\mathbf{x}}_k \tilde{\mathbf{x}}_k^H\right\} \tag{12}$$

is the extended covariance matrix and $\mathbf{0}$ is the NM-dimensional null vector.

The extended covariance matrix is estimated by

$$\hat{\mathbf{R}}_E = \begin{bmatrix} \frac{1}{K}\sum_{k=1}^{K}(\mathbf{x}_k \mathbf{x}_k^H) & \frac{1}{K}\sum_{k=1}^{K}(\alpha_k \mathbf{x}_k \mathbf{x}_k^H) \\ \frac{1}{K}\sum_{k=1}^{K}(\alpha_k \mathbf{x}_k \mathbf{x}_k^H) & \frac{1}{K}\sum_{k=1}^{K}(\alpha_k^2 \mathbf{x}_k \mathbf{x}_k^H) \end{bmatrix} \tag{13}$$

A relationship can be established between the above mentioned CME-SMI method and the DBU method by introducing the first order expansion of the covariance matrix (3) in the expectation of (13). Indeed

$$\mathbf{R}_E = \mathrm{E}\left\{\hat{\mathbf{R}}_E\right\} \tag{14}$$

$$= \frac{1}{K}\sum_{k=1}^{K}\begin{bmatrix} \mathbf{R}_{\mathrm{o}} + \alpha_k\boldsymbol{\Delta}\mathbf{R}_{\mathrm{o}} & \alpha_k\mathbf{R}_{\mathrm{o}} + \alpha_k^2\boldsymbol{\Delta}\mathbf{R}_{\mathrm{o}} \\ \alpha_k\mathbf{R}_{\mathrm{o}} + \alpha_k^2\boldsymbol{\Delta}\mathbf{R}_{\mathrm{o}} & \alpha_k^2\mathbf{R}_{\mathrm{o}} + \alpha_k^3\boldsymbol{\Delta}\mathbf{R}_{\mathrm{o}} \end{bmatrix}$$

Let $\alpha_k = \sqrt{\frac{12}{K^2-1}}\left(k - \frac{K+1}{2}\right)$ verifying $\frac{1}{K}\sum_{k=1}^{K}\alpha_k = 0$ and $\frac{1}{K}\sum_{k=1}^{K}\alpha_k^2 = 1$ to avoid the noise amplification [13], thus

$$\mathbf{R}_E = \begin{bmatrix} \mathbf{R}_{\mathrm{o}} & \boldsymbol{\Delta}\mathbf{R}_{\mathrm{o}} \\ \boldsymbol{\Delta}\mathbf{R}_{\mathrm{o}} & \mathbf{R}_{\mathrm{o}} \end{bmatrix}, \tag{15}$$

Now, by using (8), (9), (11) and (15) we find

$$\mathbf{w}_k \approx \left(\mathbf{R}_A^{-1} + \alpha_k\mathbf{R}_B^{-1}\right)\mathbf{v}_{\mathrm{t}} \tag{16}$$

where

$$\mathbf{R}_A = \mathbf{R}_{\mathrm{o}} - \boldsymbol{\Delta}\mathbf{R}_{\mathrm{o}}\mathbf{R}_{\mathrm{o}}^{-1}\boldsymbol{\Delta}\mathbf{R}_{\mathrm{o}} \tag{17}$$

and

$$\mathbf{R}_B = \boldsymbol{\Delta}\mathbf{R}_{\mathrm{o}} - \mathbf{R}_{\mathrm{o}}\boldsymbol{\Delta}\mathbf{R}_{\mathrm{o}}^{-1}\mathbf{R}_{\mathrm{o}} \tag{18}$$

A simple calculation yields:

$$\mathbf{R}_A^{-1} = (\mathbf{I} - \mathbf{R}_{\mathrm{o}}^{-1}\boldsymbol{\Delta}\mathbf{R}_{\mathrm{o}}\mathbf{R}_{\mathrm{o}}^{-1}\boldsymbol{\Delta}\mathbf{R}_{\mathrm{o}})^{-1}\mathbf{R}_{\mathrm{o}}^{-1} = \mathbf{R}_{\mathrm{o}}^{-1} + O(\boldsymbol{\Delta}\mathbf{R}_{\mathrm{o}}^2)) \tag{19}$$

and

$$\mathbf{R}_B^{-1} = -(\mathbf{I} + (\mathbf{R}_{\mathrm{o}}\boldsymbol{\Delta}\mathbf{R}_{\mathrm{o}}^{-1}\mathbf{R}_{\mathrm{o}})^{-1}\boldsymbol{\Delta}\mathbf{R}_{\mathrm{o}})^{-1}\mathbf{R}_{\mathrm{o}}^{-1}\boldsymbol{\Delta}\mathbf{R}_{\mathrm{o}}\mathbf{R}_{\mathrm{o}}^{-1} = -\mathbf{R}_{\mathrm{o}}^{-1}\boldsymbol{\Delta}\mathbf{R}_{\mathrm{o}}\mathbf{R}_{\mathrm{o}}^{-1} + O(\boldsymbol{\Delta}\mathbf{R}_{\mathrm{o}}^2)) \tag{20}$$

where $O(\boldsymbol{\Delta}\mathbf{R}_{\mathrm{o}}^2)$ means a quantity of the order of $\boldsymbol{\Delta}\mathbf{R}_{\mathrm{o}}^2$.

In first approximation, this finally yields:

$$\mathbf{w}_k \approx \left(\mathbf{I} - \alpha_k\mathbf{R}_{\mathrm{o}}^{-1}\boldsymbol{\Delta}\mathbf{R}_{\mathrm{o}}\right)\mathbf{R}_{\mathrm{o}}^{-1}\mathbf{v}_{\mathrm{t}} \tag{21}$$

The same result is obtained by a first order approximation of the inverse of the CME in (4) and by using k instead of α_k.

The difference between the CME-SMI and DBU lies in the fact that for CME-SMI $\mathbf{R}_{\text{o}}$ and $\mathbf{\Delta R}_{\text{o}}$ must be estimated with sample data as for SMI whereas for the DBU $\mathbf{R}_{\text{o}}$ and $\mathbf{\Delta R}_{\text{o}}$ are directly obtained through parts of the extended covariance matrix. We will see in the simulation section that because of the wrong estimation of the $\mathbf{R}_{\text{o}}$ and $\mathbf{\Delta R}_{\text{o}}$ matrices, the CME-SMI method performs like the SMI and is then less performant than the DBU method.

C. Taylor Subspace Expansion and eigencanceler (SE-EC)

The space time covariance matrix can be factorized as

$$\mathbf{R}_k = \mathbf{U}_k \mathbf{\Delta}_k \mathbf{U}_k^H = \mathbf{U}_{\text{c},k} \mathbf{\Delta}_{\text{c},k} \mathbf{U}_{\text{c},k}^H + \mathbf{U}_{\text{n},k} \mathbf{\Delta}_{\text{n},k} \mathbf{U}_{\text{n},k}^H \tag{22}$$

where $\mathbf{\Delta}_{\text{c},k}$ and $\mathbf{\Delta}_{\text{n},k}$ are the diagonal matrices $diag\left\{\lambda_1 \cdots \lambda_r\right\}$ and $diag\left\{\lambda_{r+1} \cdots \lambda_{NM}\right\}$ containing the eigenvalues of the clutter plus noise covariance matrix $\mathbf{R}_k$ such as $\lambda_1 \geq \cdots \geq \lambda_r > \lambda_{r+1} = \lambda_{NM} = \sigma^2$ and $\mathbf{U}_{\text{c},k}$ and $\mathbf{U}_{\text{n},k}$ are the associated eigenvectors. M and N are the number of pulses and antenna elements, respectively. r is the rank of the clutter only covariance matrix (in the absence of noise) and is given by Brennan's rule [1][2]. The subspaces spanned by $\mathbf{U}_{\text{c},k}$ and $\mathbf{U}_{\text{n},k}$ are refered to as the clutter an noise subspaces at range k, respectively. A STAP filter can be defined using the eigencanceler method [18], as

$$\mathbf{w_k} = (\mathbf{I} - \mathbf{U}_{\text{c},k} \mathbf{U}_{\text{c},k}^H) \cdot \mathbf{v}_{\text{t}} \tag{23}$$

Usually, $\mathbf{U}_{\text{c},k}$ is obtained from the estimated covariance matrix $\hat{\mathbf{R}}_k$. We here propose to combine this method with a Taylor series expansion of the interference subspace. Let $\mathbf{U} = [\mathbf{u}_1 \cdots \mathbf{u}_{NM}]$ be the $MNXMN$ dimensional matrix the columns of which span the interference plus noise subspace at range k. At a given range k, the clutter eigenvector $\mathbf{u}_{\text{c}_1}$ associated with the largest eigenvalue maximizes the following cost function

$$\mathbf{u}_{i,k}^H \mathbf{R}_k \mathbf{u}_{i,k} \quad \text{under constraint} \quad \mathbf{u}_{i,k}^H \mathbf{u}_{i,k} = 1 \tag{24}$$

The other clutter eigenvectors are found by maximizing $\forall i \in [2, NM]$ the same cost function with constraint $\mathbf{u}_{i,k}^H \mathbf{u}_{i,k} = 1$ and $\mathbf{u}_{i,k}^H \mathbf{u}_{i-1,k} = 0$ (see the Appendix for the proof and theorems

[2]The rank r of the clutter covariance matrix in the case of an ULA in SL configuration is given by $r = M + \beta(N-1)$ where $\beta = \frac{2v_{\text{a}}T_r}{\lambda}$, v_{a} is the platform velocity, T_r the pulse interval, λ the wavelength and M and N are the number of antenna sensors and the number of pulses, respectively. In the cases of ULA and UCCA in NSL configurations that will be considered in this paper, the rank can be approximated by twice the rank of the ULA-SL case.

11-13 of [19] for the origin of this result). Let us introduce a first order expansion of each eigenvector as

$$\mathbf{u}_{i,k} \approx \mathbf{u}_{o_i} + \alpha_k \boldsymbol{\Delta}\mathbf{u}_{o_i} \tag{25}$$

$\forall i \in [1, NM]$, the cost function thus becomes

$$(\mathbf{u}_{\mathrm{o}_i} + \alpha_k \boldsymbol{\Delta}\mathbf{u}_{\mathrm{o}_i})^H \mathbf{R}_k (\mathbf{u}_{\mathrm{o}_i} + \alpha_k \boldsymbol{\Delta}\mathbf{u}_{\mathrm{o}_i}) \tag{26}$$

and is to be maximized over the set of vectors $[\mathbf{u}_{\mathrm{o}_i} + \alpha_k \boldsymbol{\Delta}\mathbf{u}_{\mathrm{o}_i}]$ with $i \in [1, NM]$ under constraint

$$(\mathbf{u}_{\mathrm{o}_i} + \alpha_k \boldsymbol{\Delta}\mathbf{u}_{\mathrm{o}_i})^H (\mathbf{u}_{\mathrm{o}_i} + \alpha_k \boldsymbol{\Delta}\mathbf{u}_{\mathrm{o}_i}) = 1 \tag{27}$$

This constraint thus involves

$$\mathbf{u}_{\mathrm{o}_i}^H \mathbf{u}_{\mathrm{o}_i} + \alpha_k \left(\mathbf{u}_{\mathrm{o}_i}^H \boldsymbol{\Delta}\mathbf{u}_{\mathrm{o}_i} + \boldsymbol{\Delta}\mathbf{u}_{\mathrm{o}_i}^H \mathbf{u}_{\mathrm{o}_i} \right) + \alpha_k^2 \boldsymbol{\Delta}\mathbf{u}_{\mathrm{o}_i}^H \boldsymbol{\Delta}\mathbf{u}_{\mathrm{o}_i} = 1 \tag{28}$$

By choosing α_k so that $\frac{1}{K}\sum_{k=1}^K \alpha_k = 0$ and $\frac{1}{K}\sum_{k=1}^K \alpha_k^2 = 1$ and by summing each side of (28), it comes

$$\mathbf{u}_{\mathrm{o}_i}^H \mathbf{u}_{\mathrm{o}_i} + \boldsymbol{\Delta}\mathbf{u}_{\mathrm{o}_i}^H \boldsymbol{\Delta}\mathbf{u}_{\mathrm{o}_i} = 1 \tag{29}$$

Let $\tilde{\mathbf{u}}_i = \begin{bmatrix} \mathbf{u}_{\mathrm{o}_i} \\ \boldsymbol{\Delta}\mathbf{u}_{\mathrm{o}_i} \end{bmatrix}$ be the i^{th} extended eigenvector of $\mathbf{R}_E$ of (12), it maximizes the following cost function

$$\tilde{\mathbf{u}}_i^H \mathbf{R}_E \tilde{\mathbf{u}}_i \quad \text{under constraint} \quad \tilde{\mathbf{u}}_i^H \tilde{\mathbf{u}}_i = 1 \tag{30}$$

for $i = 1$ and with the additional constraint $\tilde{\mathbf{u}}_i^H \tilde{\mathbf{u}}_{i-j} = 0$ for $j = 1, ..., i-1$ $\forall i \in [2, 2NM]$. According to (13) and the above mentioned particular choice of α_k, one can write

$$\mathbf{R}_E = \mathrm{E}\left\{\hat{\mathbf{R}}_E\right\} = \begin{bmatrix} \mathbf{R}_k & \mathbf{0} \\ \mathbf{0} & \mathbf{R}_k \end{bmatrix} \tag{31}$$

It is worth noting that the extended matrix $\mathbf{R}_E$ has the same r eigenvalues greater than σ^2 as $\mathbf{R}_k$ but with multiplicity 2. Note that if $\mathbf{u}$ is an eigenvector of $\mathbf{R}_k$ associated with a given eigenvalue λ, the two linearly independent $2MN$-dimensional vectors $[\mathbf{u}, \mathbf{0}]^{\mathrm{T}}$ and $[\mathbf{0}, \mathbf{u}]^{\mathrm{T}}$ are eigenvectors of $\mathbf{R}_E$ associated with λ. It follows that in the absence of noise, the rank of $\mathbf{R}_E$ is $2r$ and that the extended clutter subspace is of dimension $2r$. Conversely, if a vector $\mathbf{u} = [\mathbf{u}_x, \mathbf{u}_y]^{\mathrm{T}}$ where $\mathbf{u}_x$ and $\mathbf{u}_y$ are vectors of dimension MN, is an eigenvector of the extended matrix $\mathbf{R}_E$ associated

with a given eigenvalue λ, then $\mathbf{u}_x$, $\mathbf{u}_y$ and any combination of $\mathbf{u}_x$ and $\mathbf{u}_y$ are eigenvectors of $\mathbf{R}_k$ associated with the same eigenvalue λ.

Thus, it follows that the clutter subspace associated with matrix $\mathbf{R}_k$ is, in particular, spanned by the vectors of the form

$$\hat{\mathbf{u}}_{i,k} = \mathbf{u}_{o,i} + \alpha_k \boldsymbol{\Delta}\mathbf{u}_{o,i} \tag{32}$$

where $\mathbf{u}_{o,i}$ and $\boldsymbol{\Delta}\mathbf{u}_{o,i}$ enters the partition of $\tilde{\mathbf{u}}_i$, the eigenvectors of $\mathbf{R}_E$ corresponding to the $2r$ largest eigenvalues of $\mathbf{R}_E$. Note that among these $2r$ eigenvectors only r of them are linearly independent implying that $span\left\{\hat{\mathbf{u}}_{1,k}, ..., \hat{\mathbf{u}}_{2r,k}\right\}$ is a r-dimensional subspace.

We then propose the so-called SE-EC STAP algorithm which consists in computing the MN-dimensional STAP weight vector as for the eigencanceler method in (23) but with $\hat{\mathbf{U}}_{\mathrm{c},k} = [\hat{\mathbf{u}}_{1,k} \cdots \hat{\mathbf{u}}_{2r,k}]$ instead of $\mathbf{U}_{\mathrm{c},k}$.

The SE-EC algorithm is expected to converge faster than the DBU algorithm. Indeed, the DBU requires at least a training data of $4NM$ range cells because with a shorter training data the estimated extended covariance matrix $\hat{\mathbf{R}}_E$ is not invertible. On the contrary the SE-EC algorithm which is a subspace-based method should require less training data as in [18]. Twice the dimension of the clutter subspace associated with $\hat{\mathbf{R}}_E$, it is to say about $4r$ range cells should be sufficient.

In order to evaluate the performance of the proposed SE-EC method and compare it to that of the CME-SMI and DBU, let us first introduce some examples of range dependent clutter.

III. Range dependency of the Clutter

Figure 1 represents the considered system [1]. The radar antenna is positioned on an airborne platform at the altitude h and moves with constant velocity $\mathbf{v}_{\mathrm{a}}$. The antenna contains N elements spaced by half a wavelength $d = \frac{\lambda}{2}$. M pulses are transmitted during a coherent processing interval (CPI). The ground clutter is split in rings of constant range R_c from the radar which are split themselves in N_{c} patches (here N_{c} = 360). Each clutter patch is described by its azimuth ϕ_{c} and its elevation θ_{c}. In the non side-looking configuration, the platform velocity vector $\mathbf{v}_{\mathrm{a}}$ is not aligned with the radar antenna axis involving a crab angle, ϕ_{a}. This configuration illustrates the majority of the practical cases, as for example, radars using rotating antennas, forward-looking

airborne radars, etc. Also when side-mounted antenna are used, an aircraft crab is used to mitigate the wind effects [1]. To study the properties of the clutter and exhibit a range dependency, we can observe the locus in a DD plane where the clutter is present. This is referred to the locus of the clutter ridges [1] which represent the space time repartition of the clutter power spectral density (PSD). This can also be obtained by investigating the analytical relation between the clutter Doppler frequency and spatial frequency. In the following, we are going to analyze and discuss this relation in some cases of antenna array geometries and flight configurations.

A. Uniformly spaced Linear Antenna (ULA) array

In the case of a ULA array, the clutter spatial frequency and the normalized Doppler frequency can be written [1]

$$\vartheta_{\mathrm{c}} = \frac{d \cdot cos(\theta_{\mathrm{c}})}{\lambda} sin\left(\phi_{\mathrm{c}}\right) \tag{33}$$

and

$$\varpi_{\mathrm{c}} = \frac{2v_{\mathrm{a}}T_r}{\lambda} cos\left(\theta_{\mathrm{c}}\right) sin\left(\phi_{\mathrm{c}} + \phi_{\mathrm{a}}\right) \tag{34}$$

respectively, where T_r is the pulse repetition interval (PRI). In the side-looking configuration, the crab angle $\phi_{\mathrm{a}} = 0$ and the relation between the Doppler and the spatial frequencies is linear so that

$$\varpi_{\mathrm{c}} = \frac{2v_{\mathrm{a}}T_r}{d} \vartheta_{\mathrm{c}} \tag{35}$$

In the side-looking configuration, the relation between the clutter Doppler frequency and the spatial frequency is linear and independent of the range R_{c} indicating that the locus of the clutter PSD is a straight line.

In the non side-looking configuration the relation which links the clutter spatial frequency and the normalized Doppler frequency is [3]

$$\vartheta_{\mathrm{c}} = \varpi_{\mathrm{c}} cos\left(\phi_{\mathrm{a}}\right) \pm \frac{1}{2} sin\left(\phi_{\mathrm{a}}\right) \sqrt{1 - \left(\frac{h}{R_{\mathrm{c}}}\right)^2 - 4\varpi_{\mathrm{c}}^2} \tag{36}$$

The locus of the PSD is no longer a straight line and a range dependency is observed. Consequently, the interference plus noise space time covariance matrix is also range dependent. This is illustrated in Figure 2 where the locus of the clutter ridges is composed of a set of

[3]In order to simplify the writting of the following relation, the coefficient $\frac{2v_{\mathrm{a}}T_r}{d}$ in (35) is here assumed equal to 1.

ellipses for different ranges R_{c} instead of being a straight line independent of R_{c} as in the case of an ULA in a side-looking configuration when $\phi_{\mathrm{a}} = 0^{\circ}$.

B. Uniform circularly curved antenna array (UCCA)

For the analysis, we choose to represent the array curvature through the opening angle γ (see Figure 3). The radius of the arc of circle which contains the sensors then varies with this angle through the following relation $R = (N-1)\frac{\lambda}{2\cdot\gamma}$. Thus, the smaller the angle γ the weaker the array curvature and the larger the radius. On the contrary, the wider the opening angle γ the larger the array curvature. The space-time steering vector is defined as the Kronecker product (here noted $\otimes$) between the temporal steering vector $\mathbf{b}(\varpi_{\mathrm{c}})$ and the spatial steering vector $\mathbf{a}(\phi_{\mathrm{c}}, \theta_{\mathrm{c}})$

$$\mathbf{v}\left(\varpi_{\mathrm{c}}, \phi_{\mathrm{c}}, \theta_{\mathrm{c}}\right) = \mathbf{b}(\varpi_{\mathrm{c}}) \otimes \mathbf{a}(\phi_{\mathrm{c}}, \theta_{\mathrm{c}}) \tag{37}$$

The n^{th} component of the spatial steering vector in (37) is defined as

$$\mathbf{a}_n(\phi_{\mathrm{c}}, \theta_{\mathrm{c}}) = e^{j\frac{2\pi}{\lambda}\cdot\mathbf{k}(\phi_{\mathbf{c}},\theta_{\mathbf{c}})\cdot\mathbf{d}_n} \tag{38}$$

where $\mathbf{k}$ is the unit vector pointing in the $(\phi_{\mathrm{c}}, \theta_{\mathrm{c}})$ direction and is given by:

$$\mathbf{k}(\phi_{\mathrm{c}}, \theta_{\mathrm{c}}) = cos(\theta_{\mathrm{c}})sin(\phi_{\mathrm{c}})\mathbf{x} + cos(\theta_{\mathrm{c}})cos(\phi_{\mathrm{c}})\mathbf{y} + sin(\theta_{\mathrm{c}})\mathbf{z} \tag{39}$$

$\mathbf{d}_n = d_{nx}\mathbf{x} + d_{ny}\mathbf{y}$ is the position vector of the n^{th} element in the $(\mathbf{x}, \mathbf{y}, \mathbf{z})$ cartesian coordinate system (we here consider a planar antenna $d_{nz} = 0\ \forall n$). We thus obtain

$$\mathbf{a}_n(\phi_{\mathrm{c}}, \theta_{\mathrm{c}}) = e^{j\frac{2\pi}{\lambda}\cdot(d_{nx}\cdot cos(\theta_{\mathbf{c}})sin(\phi_{\mathbf{c}})+d_{ny}\cdot cos(\theta_{\mathbf{c}})cos(\phi_{\mathbf{c}}))} \tag{40}$$

Referring to Figure 3, the coordinates of the antenna radar elements are given $\forall n \in [1; N]$ by

$$d_{nx} = R \cdot sin\left(\frac{\gamma}{2}\right) + R \cdot sin\left(\frac{\gamma}{N-1}\left(-\frac{N-1}{2} + (n-1)\right)\right) \tag{41}$$

$$d_{ny} = \sqrt{\left(2R \cdot sin\left(\frac{(n-1)\gamma}{2(N-1)}\right)\right)^2 - d_{nx}^2} \tag{42}$$

The temporal steering vector is the same as in the ULA case (34). However, with a UCCA array, we cannot analytically define a spatial frequency as for the ULA. In [20] and [21] a virtual spatial steering vector has been introduced but it appears that this model is not accurate when the angular extent of the UCCA is large. A more general approach has been proposed in [22]. In fact, according to this interesting work, the three normalized spatial frequencies ϑ_{cx}, ϑ_{cy}, ϑ_{cz} may

be used in a general model for all types of antenna geometries, even in the ULA case. Following [22], there exists a unique 4D-DD curve in the 4D space spanned by $\{\vartheta_{\mathrm{c}x}, \vartheta_{\mathrm{c}y}, \vartheta_{\mathrm{c}z}, \varpi_{\mathrm{c}}\}$ which represents the dependencies between the four normalized frequencies and which only depends on the scenario configuration (monostatic, bistatic, etc.). This 4D-DD curve can be projected into appropriate subspaces to deal with the particular cases of array geometries. A given antenna array may only sense a subset of this 4DD curve. As an illustration, one can see, on Figures 4 and 5, 3D and 2D projections of the 4D-DD curves corresponding to a monostatic configuration with crab angle equal to zero and to 10 deg, respectively, and for different ranges. The first remark is that the locus of the clutter ridges of figure 2 corresponds to the 2D projection $\{\vartheta_{\mathrm{c}x}, \varpi_{\mathrm{c}}\}$ of the 4D-DD curve 4 since the ULA antenna can only sense this subset. The second remark is that even in the ULA case, the relation between the spatial and the Doppler frequencies is range dependent. However, in the case of the ULA in a side looking configuration (crab angle equal to zero) the locus of the clutter ridges which can be sensed is always on the same line.

C. The bistatic case

Our motivation is to investigate the performance of our proposed algorithm in range depending clutter characteristics. In the simulation part we will also test our algorithm in some bistatic configurations. In order to exhibit the range dependency of the locus of the clutter ridges of the bistatic cases with a ULA array, we only give here the 2D projections on $\{\vartheta_{\mathrm{c}x}, \varpi_{\mathrm{c}}\}$ of the 4D-DD curves to exhibit the range dependency. Three configurations inspired by [23] are here considered the characteristics of which are given in Table I in the simulation section. The transmitter and the receiver are on two different platforms which have different trajectories. Case A is the "in trail" configuration where the transmitter and the receiver have aligned trajectories. Case B is the "wing-to-wing" configuration where the transmitter and the receiver have parallel trajectories. Case C is the orthogonal configuration where the transmitter and the receiver have orthogonal trajectories. The locus of the clutter ridges in the $\{\vartheta_{\mathrm{c}x}, \varpi_{\mathrm{c}}\}$ plane and its range dependence can be seen for cases A, B and C on Figures 6(a), 6(b) and 6(c), respectively.

In the following section, the Taylor series expansion-based algorithms presented in section II are tested and compared in these cases of range non stationarity of the data.

IV. SIMULATION RESULTS

In this section, simulation results illustrate the performance of the Taylor series expansion-based methods presented in section II. Particularly, the proposed SE-EC STAP algorithm is compared to the optimal STAP, the SMI, the diagonal loading [1], the EC [18] and the DBU [13] algorithms. This comparison concerns the performance in term of signal to interference plus noise ratio loss (SINR loss) at range k defined as the ratio of the SINR to the SNR (without clutter)

$$SINR_{loss_k} = \frac{\sigma^2 \cdot \left|\mathbf{w}_k^H \cdot \mathbf{v}_\mathrm{t}\right|^2}{NM \cdot \mathbf{w_k}^H \cdot \mathbf{R}_k \cdot \mathbf{w}_k} \tag{43}$$

where $\mathbf{w}_k$ is the weight vector of the clutter rejection filter calculated at range k according to each algorithm. At this range, the optimum SINR loss is

$$SINR_{loss_{opt_k}} = \frac{\sigma^2 \cdot \mathbf{v}_\mathrm{t}^H \cdot \mathbf{R}_k^{-1} \cdot \mathbf{v}_\mathrm{t}}{NM} \tag{44}$$

For the analysis, a pulsed Doppler airborne monostatic X-band radar composed of a uniform planar array of ULA or UCCA is considered in SL and NSL configurations. The number of radar antenna sensors in these examples is chosen equal to 12 ($N = 12$) and 10 pulses ($M = 10$) are transmitted during a CPI. The platform is assumed to move with a constant velocity of $100m.s^{-1}$ at the altitude of 9000m. The clutter to noise ratio (CNR) is assumed equal to 30 dB. The back lobe clutter is attenuated by 30 dB with respect to the front lobe clutter.

One drawback of the proposed method is that it requires the knowledge of the rank of the covariance matrix. However this rank is theoretically known only for a monostatic, side-looking configuration with a ULA antenna array. Indeed, in this case, Brennan's rule [5] indicates that the rank is $r = N + \beta(M-1)$ where $\beta = \frac{2v_\mathrm{a}T_r}{\lambda}$, v_a is the platform velocity, T_r the pulse interval and λ the wavelength. One can see on Figure 7 the eigenvalues of the clutter plus noise covariance matrix for : a) a ULA monostatic configuration for different crab angles ; b) a circular monostatic configuration for different curvature angles ; c) the ULA bistatic configurations of cases A, B and C. It appears that Brennan rule is valid only in the ULA, monostatic, side looking configuration which corresponds to the maximum of redundancy in the clutter components. In all the other cases, we will approximate the rank by $2r$[4].

[4]In eigen-based methods, an overestimation of the rank is often preferred to an underestimation since in this case the actual clutter subspace remains included in the estimated clutter subspace whereas it is not the case when the rank is underestimated

Figures 8(a) and 8(b) compare the SINR loss performance of the considered methods in the case of a ULA used in a monostatic forward-looking configuration where the crab angle is $\phi_{\text{a}} = 90°$. In Figure 8(a) the number of snapshots for estimating the covariance matrices $\mathbf{R}_E$ and $\mathbf{R}_k$ with (13) and (1), respectively, is equal to $K = 480$. It is well known that, in the case of a ULA in a side-looking configuration, the SMI converges to a SINRloss of 3 dB compared to the optimal STAP when the number of snapshots is at least $K = 2NM$. It follows that the required number of snapshots for the CME-SMI and the DBU algorithms is at least $K = 2NM$ and $K = 4NM$, respectively. In our case of $M = 12$ and $N = 10$, $K = 480$ is then an adequate choice. Thus, one can see on Figure 8(a) that the loss of performance of the SMI and the CME-SMI compared to the optimal STAP is due to the non side-looking configuration involving a range non stationarity of the snapshots. As expected, one can see that the DBU method correctly compensates for this range non stationarity. Let us note that the conventional EC algorithm as well as the diagonal loading version of the SMI also perform poorly. It is also worth noting that, as expected, the CME-SMI method performs like the SMI algorithm showing that, here, the TSE of the covariance matrix does not allow the mitigation of the range non stationarity. Indeed, the estimation of the matrices $\mathbf{R}_{\text{o}}$ and $\mathbf{\Delta R}_{\text{o}}$ required in (6) is not satisfactory since it requires the estimation of the same covariance matrix as for the SMI with the same number of snapshots and then suffers from the same drawback.

At last, it is apparent that the proposed SE-EC algorithm succeeds to compensate the range non stationarity at least as well as the DBU algorithm. Now by considering Figure 8(b) where the number of snapshots is now $K = 240$ which is not enough for the DBU algorithm, one can see that the proposed SE-EC algorithm is the only one capable of mitigating the range non stationarity involved by the forward-looking configuration. Figure 9 is another representation of the effectiveness of the proposed SE-EC algorithm compared to the SMI and DBU methods in the Doppler-Range plane when only 240 range cells are used to estimate the clutter plus noise covariance matrix.

Let us now consider the case of a UCCA antenna array with an opening angle of $\gamma = 60^o$ in a non side-looking configurations of crab angle $\phi_{\text{a}} = 10°$. In the case of the UCCA, the non side looking configuration is here defined when there is a non zero crab angle between the speed

Case	x_R	y_R	y_R	α_R	v_T	v_R	R_{test}
A	20	0	0	0	100	100	35
B	0	20	0	0	100	100	35
C	0	20	0	90	100	100	35

TABLE I

CHARACTERISTICS OF THE BISTATIC CONFIGURATIONS. x_R, y_R, z_R AND R_{test} ARE EXPRESSED IN KM, α_R IN DEGREES AND v_T AND v_R IN M/S.

direction of the airplane and the axis joining the two extreme antennas of the array, i.e. axis (O, x) as it can be seen on Figure 3. As in the case of the ULA, we can see that the DBU and the proposed SE-EC STAP algorithms are capable of compensating the range non stationarity involved by both the non ULA and the non side-looking configurations when the number of snapshots is $K = 4NM = 480$ while only the proposed SE-EC algorithm can do it for $K = 240$ snapshots. Also note that even in the first case, the SE-EC algorithm outperforms the DBU method. It thus appears that the proposed SE-EC algorithm outperforms the other algorithms and requires less range cells to converge than the DBU algorithm.

Another illustration of the interest of the proposed SE-EC algorithm is exhibited in the bistatic configurations the characteristics of which are given in Table I. These characteristics are the coordinates (x_R, y_R, z_R) of the receiver airborne platform with respect to the transmitter airborne platform, the angle between the directions of the two airborne platforms, the velocity of the platforms and the range of the cell under test.

V. CONCLUSION

We have investigated the use of the Taylor series expansion of the space time covariance matrix and of the interference subspace in STAP in order to mitigate a possible range non stationarity of the data which may occur in the cases of non ALU antenna arrays, non side-looking configurations, non homogeneous clutter and bistatic configurations. The new SE-EC algorithm has been proposed and a relation between the DBU and the CME-SMI algorithms has

been established. The performance of these algorithms have been compared by simulations in the cases of a ULA and a UCCA in monostatic side- and non side-looking configurations and in some cases of bistatic configurations. The proposed SE-EC algorithm outperforms the other algorithms, with a comparable complexity to the DBU algorithm ($O\left((2NM)^3\right)$) but requires less range cells to obtain better results.

ACKNOWLEDGEMENT

The authors are very grateful to the anonymous reviewers whose comments were very useful to improve this paper.

APPENDIX

Let $\mathbf{R}$ be a complex, Hermitian matrix of dimension P. Maximizing the quadratic function

$$\mathbf{u}^H\mathbf{R}\mathbf{u} \tag{45}$$

under constraint :

$$\mathbf{u}^H\mathbf{u} = 1 \tag{46}$$

is equivalent to maximizing :

$$J(\mathbf{u}) = \mathbf{u}^H\mathbf{R}\mathbf{u} + \lambda(\mathbf{u}^H\mathbf{u} - 1) \tag{47}$$

where $\mathbf{u}$ is a complex vector of dimension P and λ is a Lagrange multiplier. This maximization problem yields the solution $\mathbf{u}_1$:

$$\mathbf{R}\mathbf{u}_1 = -\frac{\lambda}{2}\mathbf{u}_1 = \mu_1\mathbf{u}_1 \tag{48}$$

This means that the solution $\mathbf{u}_1$ is an eigenvector of $\mathbf{R}$ associated with the eigenvalue μ_1. As $\mathbf{u}_1$ maximizes (45) under constraint (46), it follows that :

$$\mathbf{u}_1^H\mathbf{R}\mathbf{u}_1 = \mu_1\mathbf{u}_1^H\mathbf{u}_1 = \mu_1 = \mu_{\max}$$

the largest eigenvalue of matrix $\mathbf{R}$.

Let us now consider the maximization of the same quadratic function (45) under the two constraints :

$$\mathbf{u}^H\mathbf{u} = 1 \tag{49}$$

and

$$\mathbf{u}^H\mathbf{u}_1 = 0 \tag{50}$$

where $\mathbf{u}_1$ is the vector maximizing the first problem. By using the Lagrange multipliers λ_1 and λ_2, the new problem is equivalent to maximizing :

$$J(\mathbf{u}) = \mathbf{u}^H\mathbf{R}\mathbf{u} + \lambda_1(\mathbf{u}^H\mathbf{u} - 1) + \lambda_2\mathbf{u}^H\mathbf{u}_1 \tag{51}$$

The solution of this problem $\mathbf{u}_2$ is solution of the following equation :

$$2\mathbf{R}\mathbf{u}_2 + \lambda_1\mathbf{u}_2 + \lambda_2\mathbf{u}_1 = 0 \tag{52}$$

Now by multiplying on the left by the transconjugate of $\mathbf{u}_1$ which is an eigenvector of $\mathbf{R}$ associated with the largest eigenvalue of $\mathbf{R}$, $\mu_{\max}$, and taking into account that $\mathbf{R}$ is Hermitian gives :

$$2\mathbf{u}_1^H\mathbf{R}\mathbf{u}_2 + \lambda_2\mathbf{u}_1^H\mathbf{u}_1 = 2\mu_{\max}\mathbf{u}_1^H\mathbf{u}_2 + \lambda_2 = 0 \tag{53}$$

which means, according to (50) that $\lambda_2 = 0$. Consequently,

$$\mathbf{R}\mathbf{u}_2 = -\frac{\lambda_1}{2}\mathbf{u}_2 = \mu_2\mathbf{u}_2 \tag{54}$$

which implies that $\mathbf{u}_2$ is an eigenvector of $\mathbf{R}$ associated with the eigenvalue μ_2. Now, as $J(\mathbf{u})_{\max}$ of (51) is equal to $J(\mathbf{u}_2) = \mathbf{u}_2^H\mathbf{R}\mathbf{u}_2 = \mu_2$, it follows that μ_2 is the largest eigenvalue $\mu_{\max}$ or the second largest eigenvalue if $\mu_{\max}$ is of multiplicity 1. More generally, let us denote by $\mathbf{u}_j$ a vector maximizing the quadratic function (45) under the constraint (49) and:

$$\mathbf{u}^H\mathbf{u}_i = 0 \quad \text{for} \quad i = 1, \ldots, j-1 \tag{55}$$

where the $\mathbf{u}_i$, for $i = 0, \ldots, j-1$, are the $j-1$ normalized and orthogonal eigenvectors associated with the $j-1$ largest eigenvalues $\mu_1 \geq \mu_2 \geq \ldots \mu_{j-1}$. Following the same idea as above, vector $\mathbf{u}_j$ is a normalized eigenvector associated with the jth largest eigenvalue μ_j after the $j-1$ already obtained eigenvalues.

REFERENCES

[1] J. Ward, "Space-Time Adaptive Processing for airborne radar,"*Technical Report 1015*, Lincoln Laboratory MIT, Dec. 1994.

[2] R. Klemm, "Principles of Space-Time Adaptive Processing", *IEE Radar, Sonar, Navigation and Avionics*, 12, 2002.

[3] JR. Guerci, "Space-Time Adaptive Processing for Radar," *Artech House*, 2003.

[4] W.L. Melvin, "A STAP overview," *IEEE AES Magazine-Special Tutorials Issue*, 19,1, pp. 19-35, 2004.

[5] I.S. Reed, J.D. Mallet and L.E. Brennan, "Rapid convergence rate in adaptive arrays," *IEEE Trans. on Aerospace and Electronic Systems*, 10,6, pp. 853–863, 1974.

[6] G. Borsari, "Mitigating effects on STAP processing caused by an inclined array" in *Proceedings of the IEEE Radar Conference*, Dallas, Texas, pp. 135–140, 1998.

[7] M. Zatman, "Circular array STAP" *IEEE Trans. on Aerospace and Electronic Systems*, 36, 2, pp. 510–517, 2000.

[8] R. Klemm, "Ambiguities in bistatic STAP radar", in *Proceedings of IEEE International Geoscience and Remote Sensing Symposium*, Honolulu, Hawai, 3, 2000.

[9] S.M. Kogon and M.A. Zatman, "Bistatic STAP for airborne radar systems," in *Proceedings of IEEE SAM*, Lexington, MA, 2000.

[10] B. Himed, Y. Zhang and A. Hajjari "STAP with angle-Doppler compensation for bistatic airborne radars," in *Proceedings of the IEEE Radar Conference*, Long Beach, CA, pp. 311–317, April 2002.

[11] W.L. Melvin, B. Himed and M.E. Davis, "Doubly-adaptive bistatic clutter filtering," in *Proceedings of the IEEE Radar Conference*, pp. 171–178, 2003.

[12] WL. Melvin and ME. Davis, "Adaptive cancellation method for geometry-induced nonstationary bistatic clutter environments,"in *IEEE Transactions on Aerospace and Electronic Systems*, 43, 2, pp. 651–672, 2007.

[13] M.Zatman, "Performance Analysis of the Derivative Based Updating Method," in *Proceedings of the IEEE Adaptive Sensor Array Processing (ASAP) workshop*, Lexington, MA, 2001.

[14] C.H. Lim and B. Mulgrew, "Linear prediction of range-dependent inverse covariance matrix (PICM) sequences", *Signal Processing*,87(6), pp. 1412-1420, 2007.

[15] F.D. Lapierre, J.G. Verly and M. Van Droogenbroeck, "New solutions to the problem of range dependence in bistatic STAP radars," in *Proceedings of the IEEE Radar Conference*, Huntsville, AL, pp. 452-459, 2003.

[16] F.D. Lapierre and J.G. Verly, "Registration-based range-dependence compensation for bistatic STAP radars," in *EURASIP Journal on Applied Signal Processing*, vol. 1, pp. 85 - 98, Jan 2005.

[17] D.J. Rabideau, "Taylor series adaptive processing,", in Proceedings of the Tenth IEEE Workshop on Statistical Signal and Array Processing, 2000.

[18] A.Haimovich, "The eigencanceler: adaptive radar by eigenanalysis methods," in *IEEE Transactions on Aerospace and Electronic Systems*, vol. 32, pp. 532–542, Apr 1996.

[19] F.R. Gantmacher, "Theorie des matrices", tome 1, (french translation of the original Russian version) Dunod, 1966.

[20] M. Bhren et al., "Virtual Array Design for Array Interpolation using Differential Geometry," in *IEEE International Conference on Acoustics, Speech, and Signal Processing*, vol. 2, pp. 229–232, May 2004.

[21] P. Ries et al., Array Interpolation Applied to Conformal Array STAP, in Proceedings of the IEEE BENELUX/DSP Valley Signal Processing Symposium, 2005.

[22] P. Ries, X. Neyt, F.D. Lapierre and J.G. Verly, Fundamental of spatial and Doppler frequencies in radar STAP, in IEEE Transactions on Aerospace and Electronics Systems, 2008.

[23] F.D. Lapierre, Registration-based range-dependence compensation in airborne bistatic radar STAP, PhD thesis, University of Lige, Belgium, Nov. 2004.

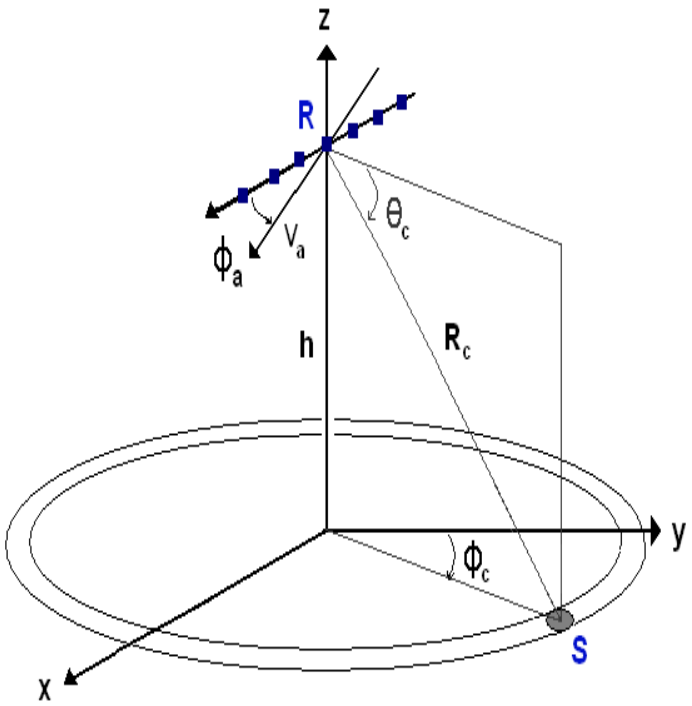

Fig. 1. Geometry of the monostatic non side-looking configuration

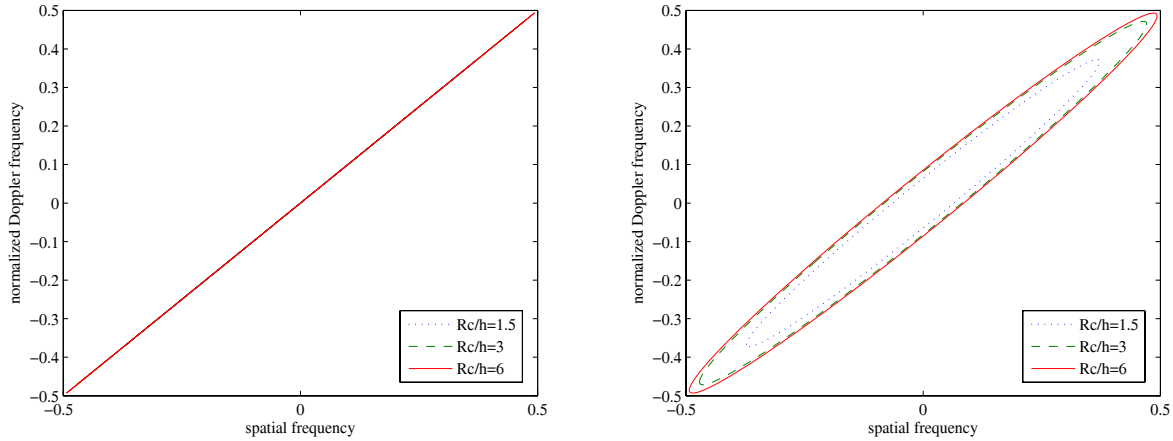

(a) (b)

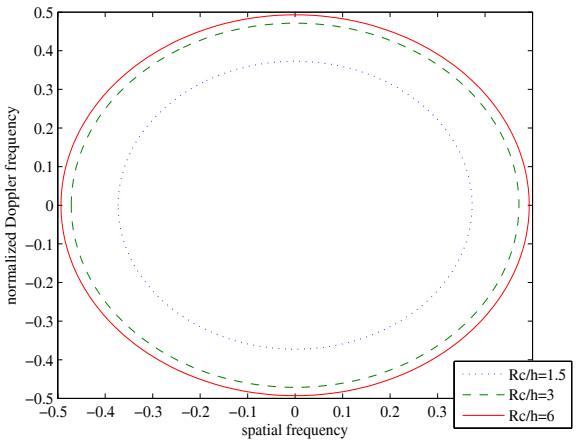

(c)

Fig. 2. Examples of the locus of clutter ridges in case of an ULA in monostatic configuration. (a) crab angle of $\phi_a = 0^o$; (b) crab angle of $\phi_a = 10^o$; (c) crab angle of $\phi_a = 90^o$

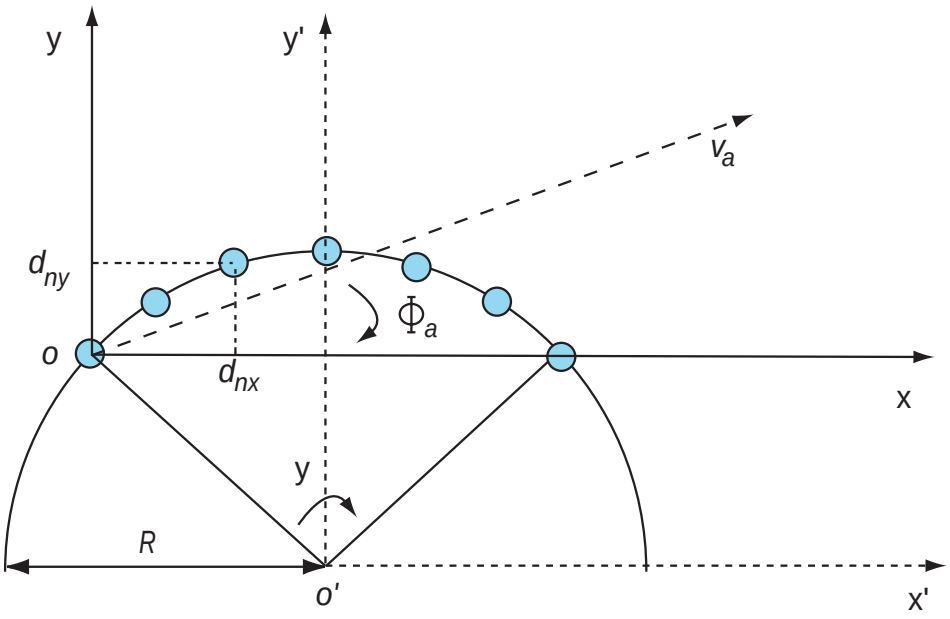

Fig. 3. Top view of the uniform circularly curved antenna (UCCA) array

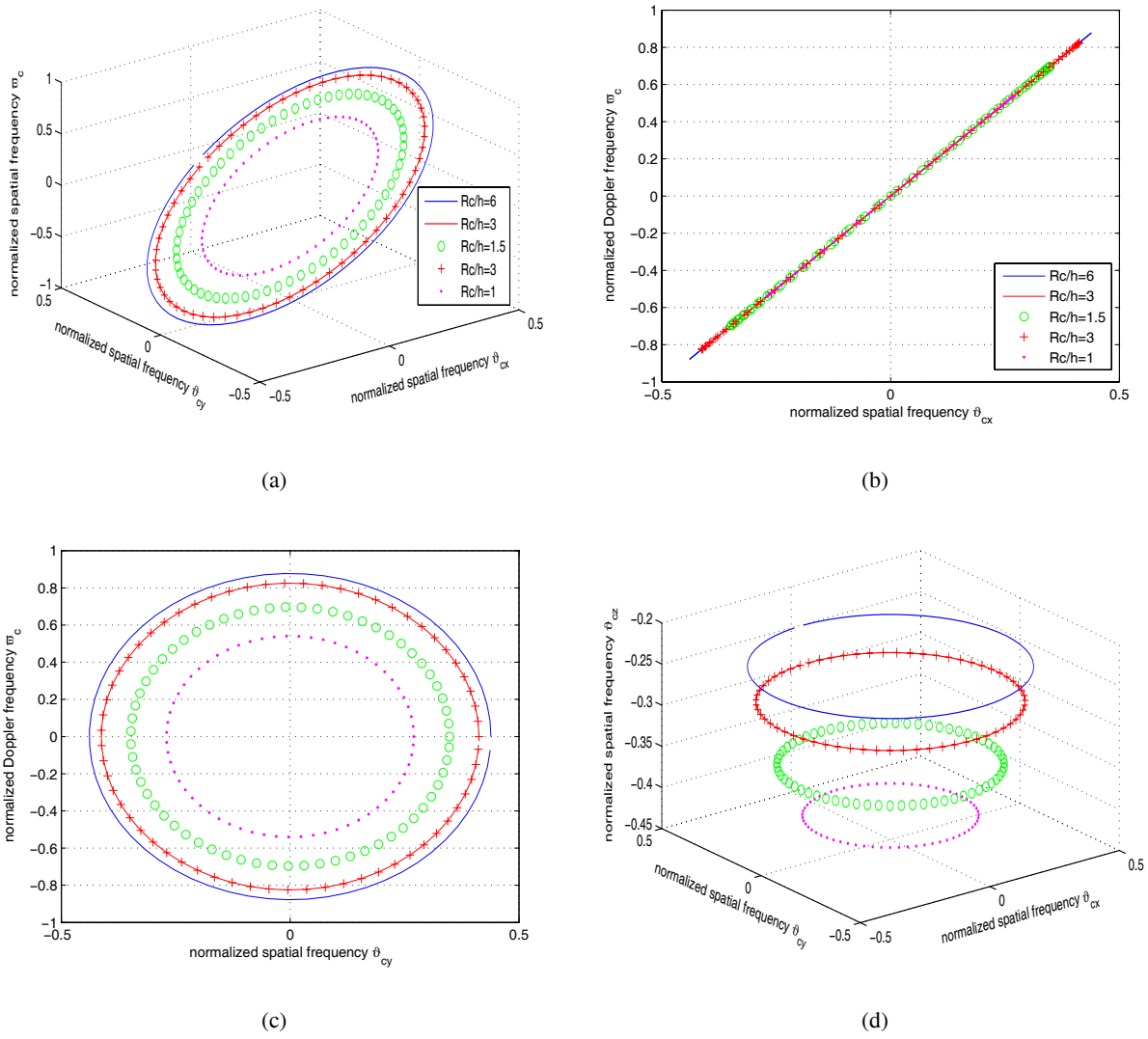

Fig. 4. Representation of the 4D-DD curve through 2D and 3D projections. Monostatic configuration. $\phi_a = 0^o$

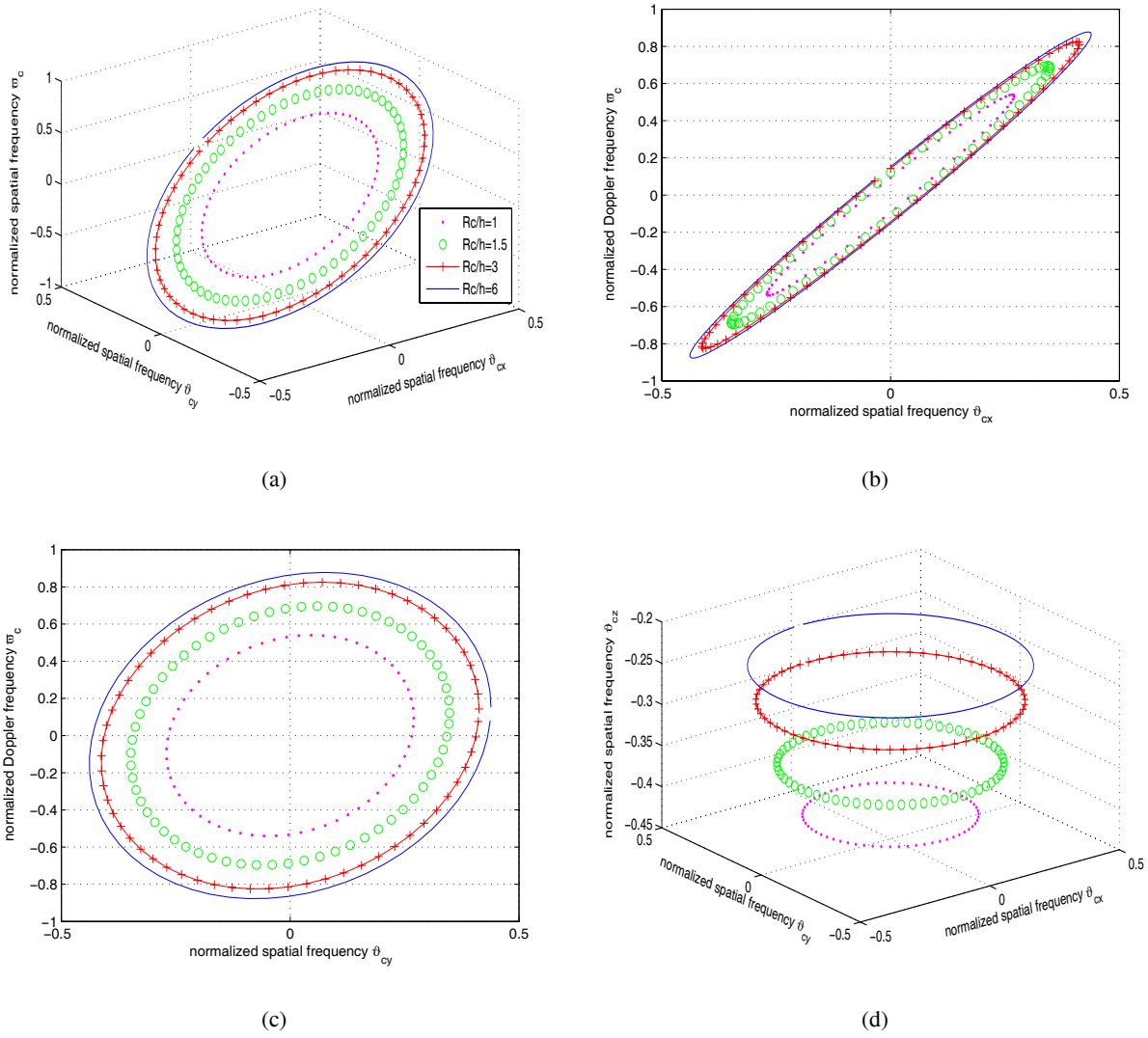

Fig. 5. Representation of the 4D-DD curve through 2D and 3D projections. Monostatic configuration. $\phi_a = 10^o$

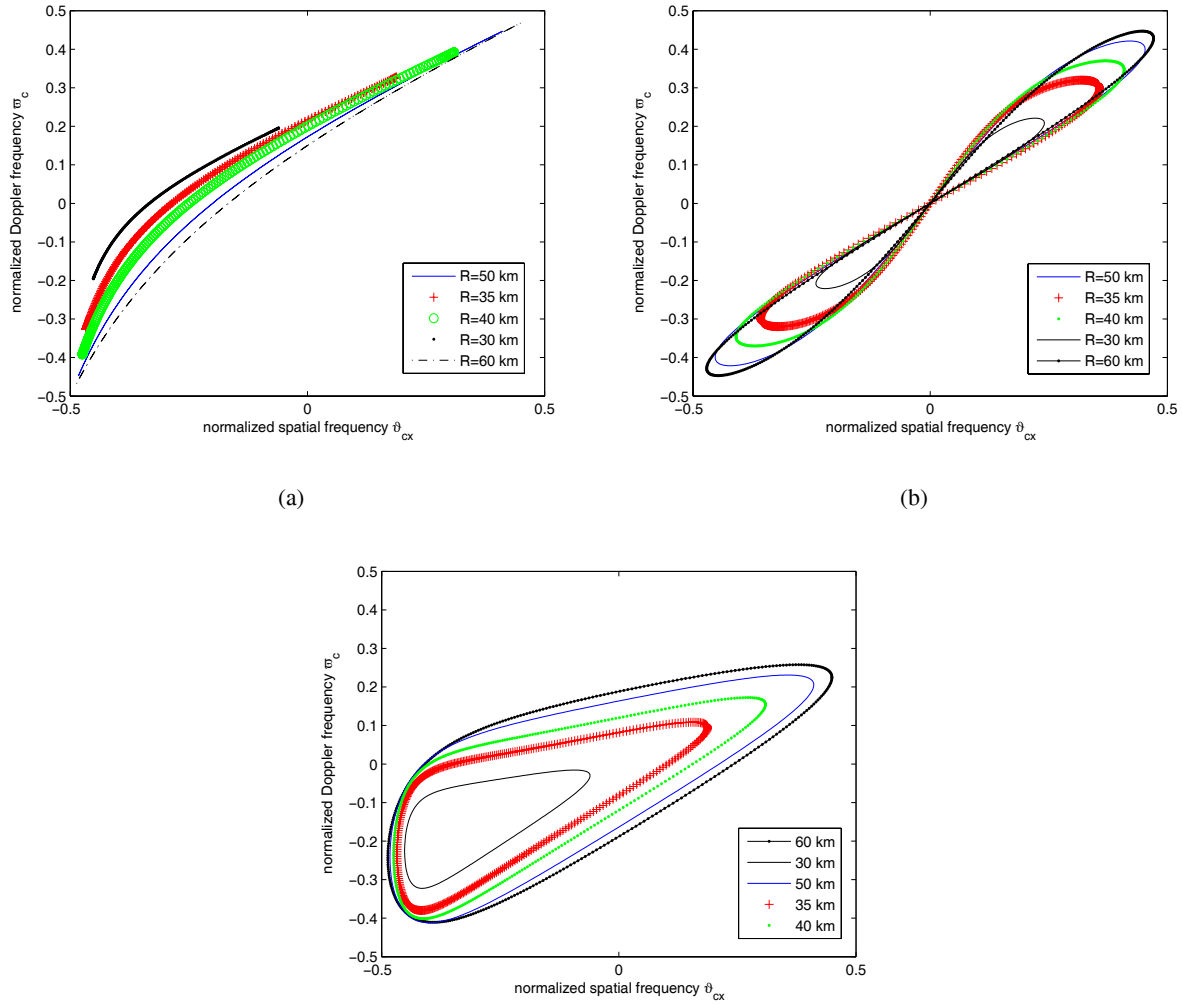

Fig. 6. DD curves in the (ϑ, ϖ) plane for different bistatic configurations and ranges. a) Case A : in trail configuration, b) Case B : wing-to-wing configuration, c) Case C : orthogonal configuration. See Table I for the characteristics.

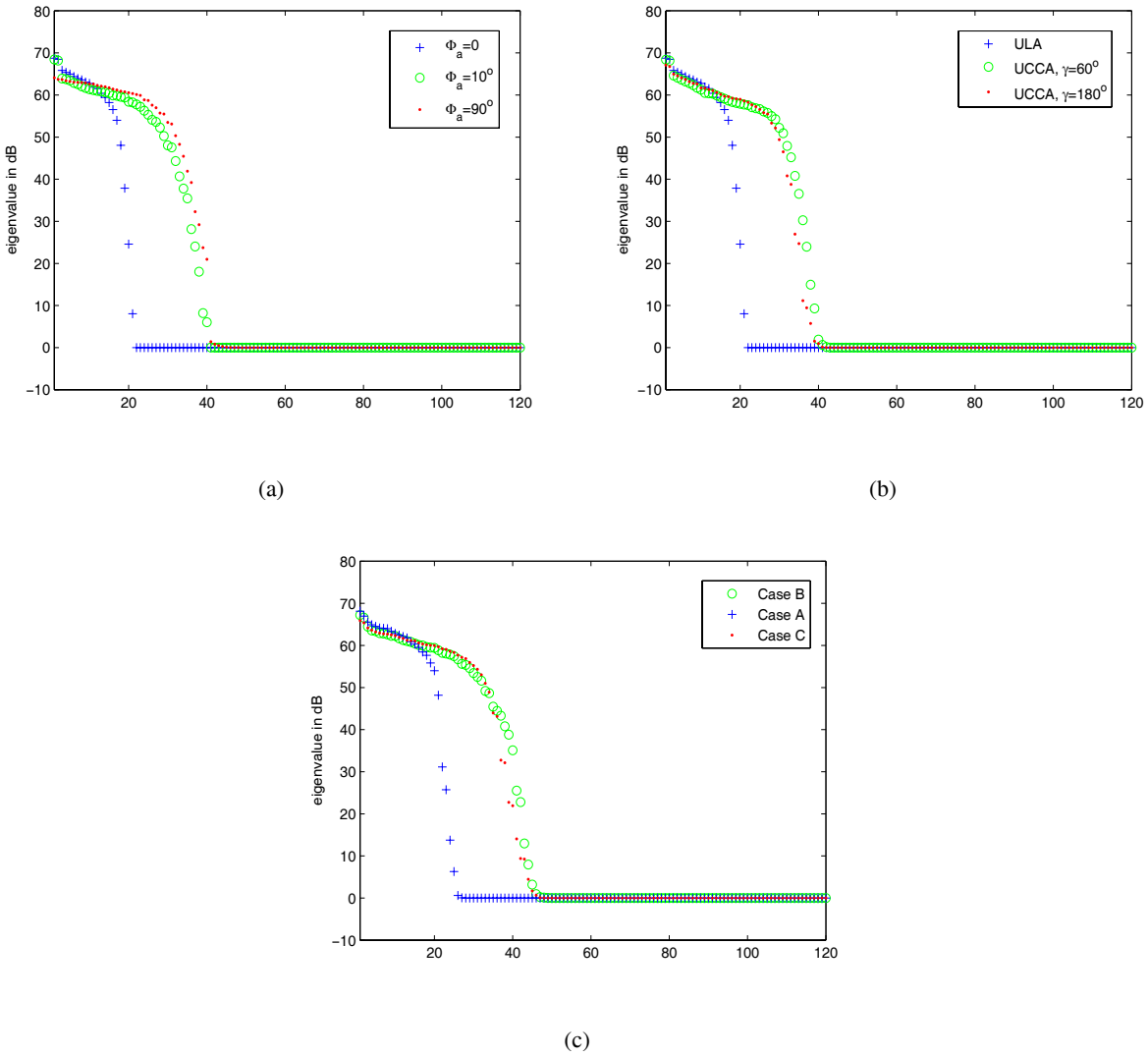

Fig. 7. Eigenvalues of the clutter plus noise covariance matrix. a) Monostatic configuration with ULA for different crab angles ; b) Monostatic configuration with UCCA for different curvature angles ; c) Bistatic configuration for cases A, B and C.

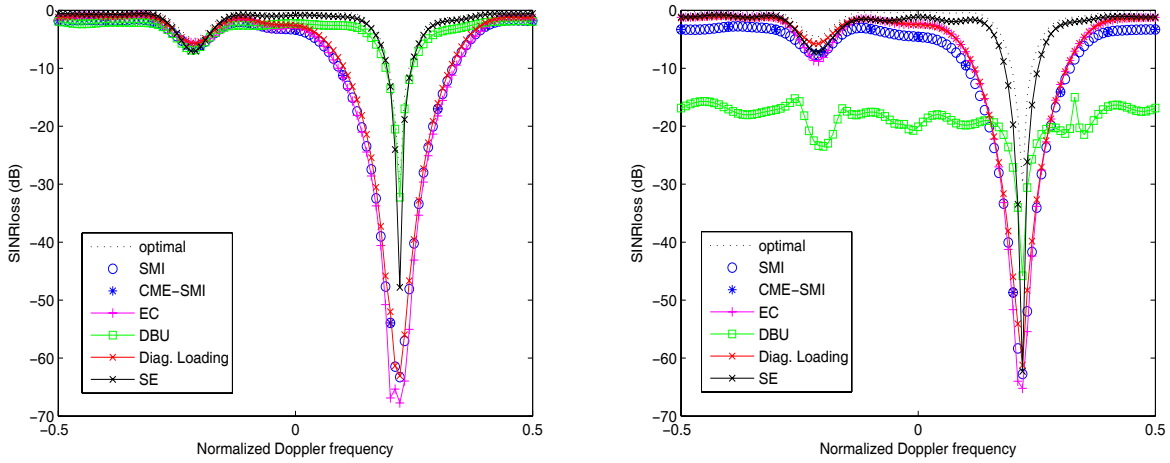

(a) (b)

Fig. 8. Slice of $SINR_{loss}$ in dB: Case of an ULA in a monostatic forward-looking configuration with training data of (a) 480 range cells ; and (b) 240 range cells

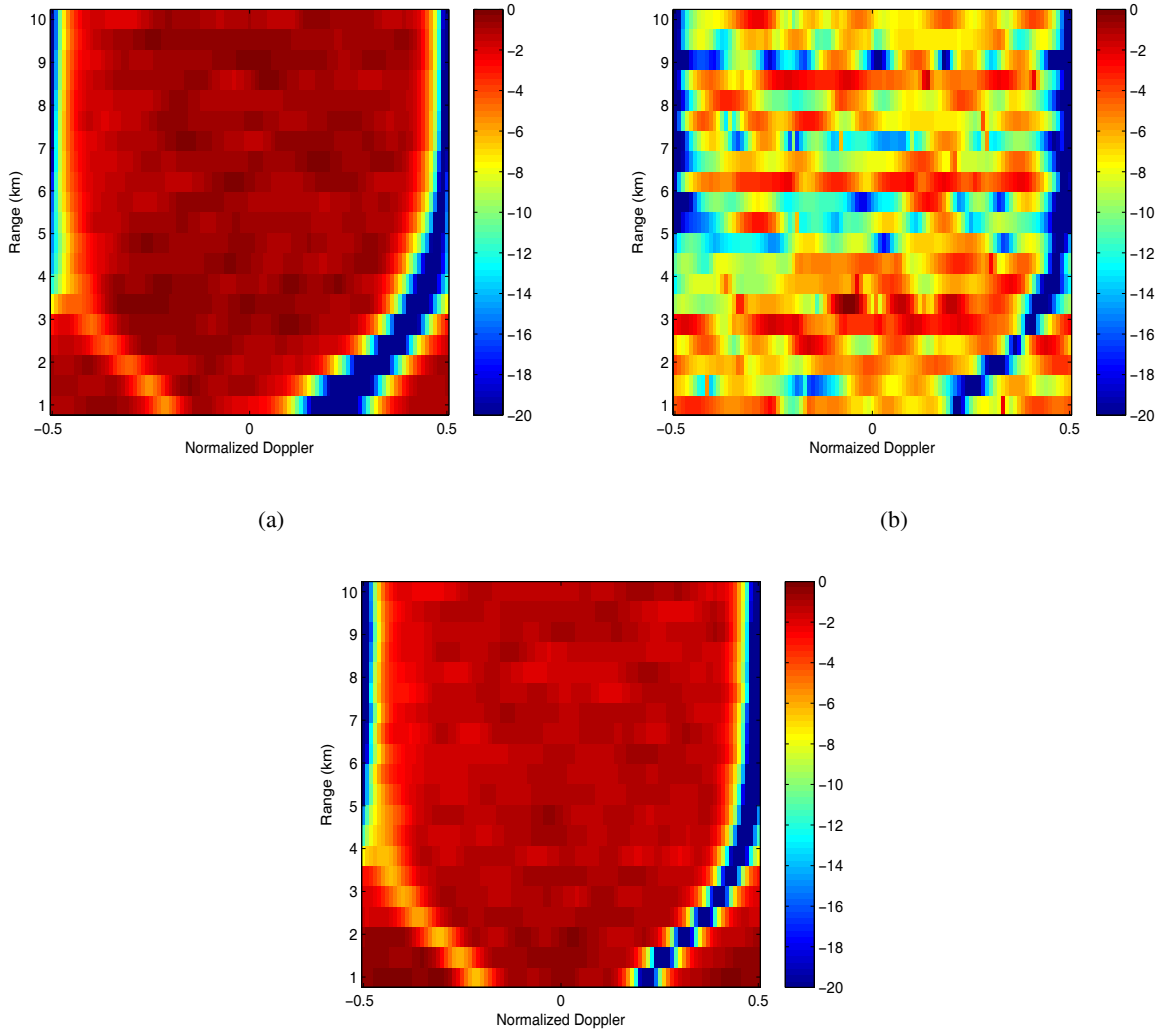

Fig. 9. Doppler range representation of the clutter suppression. a) SMI ; b) DBU ; c) SE. 240 snapshots.

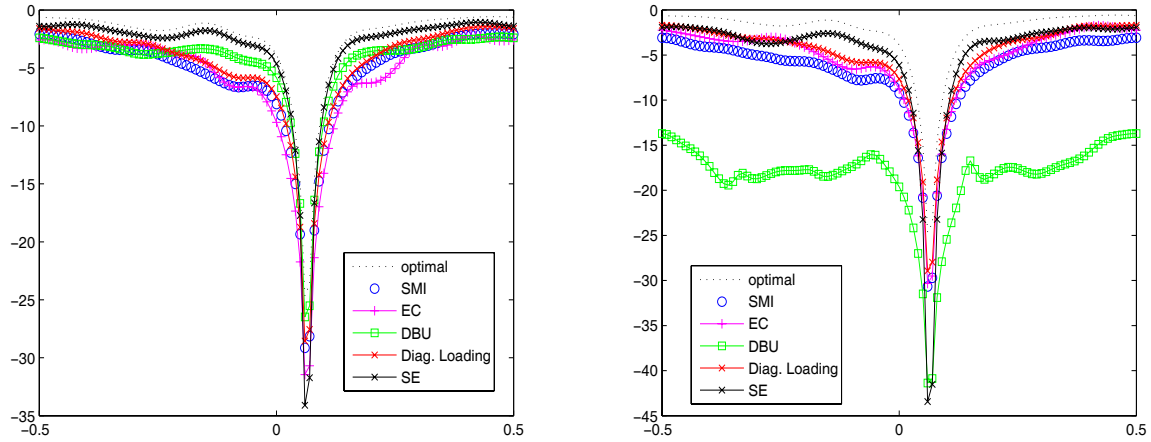

(a) (b)

Fig. 10. Slice of $SINR_{loss}$ in dB: Case of an UCCA (opening angle $\gamma = 60^o$) in a monostatic non side looking configuration) with a crab angle of 10^o with training data of (a) 480 range cells and (b) 240 range cells

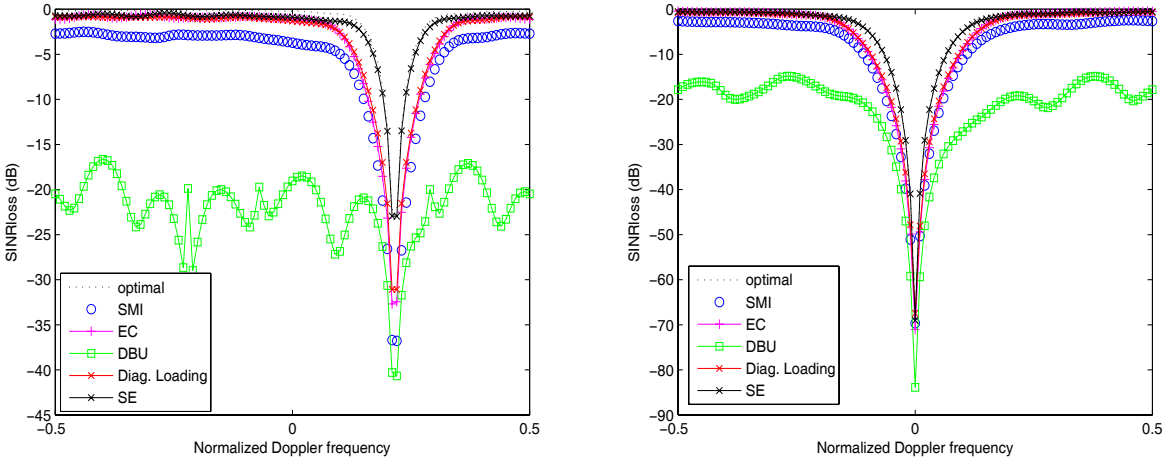

(a) (b)

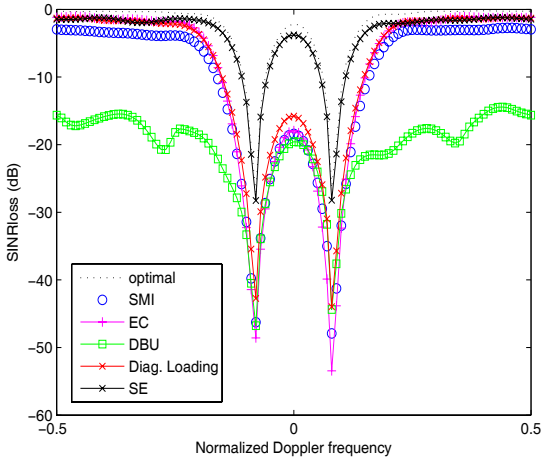

(c)

Fig. 11. Slice of $SINR_{loss}$ in dB: Case of an ULA in bistatic configurations. a) case A, b) case B, c) case C. Training data of 240 range cells